IOPscience iopscience.iop.org

Home Search Collections Journals About Contact us My IOPscience

Free carrier mobility in AlGaN/GaN quantum wells

This article has been downloaded from IOPscience. Please scroll down to see the full text article.

2002 J. Phys.: Condens. Matter 14 13319

(http://iopscience.iop.org/0953-8984/14/48/384)

View the table of contents for this issue, or go to the journal homepage for more

Download details:
IP Address: 171.66.16.97
The article was downloaded on 18/05/2010 at 19:17

Please note that terms and conditions apply.

INSTITUTE OF PHYSICS PUBLISHING JOURNAL OF PHYSICS: CONDENSED MATTER

J. Phys.: Condens. Matter **14** (2002) 13319–13328 PII: S0953-8984(02)54175-8

Free carrier mobility in AlGaN/GaN quantum wells

J-L Farvacque[1,4], Z Bougrioua[2], F Carosella[1] and I Moerman[3]

[1] Laboratoire de Structure et Propriétés de l'Etat Solide, CNRS ESA 8008, Université des Sciences et Technologies de Lille, 59655 Villeneuve d'Ascq Cedex, France
[2] CHREA-CNRS, rue Bernard Gregory, 06560 Valbonne, France
[3] INTEC, IMEC vzw-Ghent University, Sint-Pietersnieuwstraat 41, B-9000 Ghent, Belgium

E-mail: Jean-Louis.Farvacque@univ-lille1.fr

Received 27 September 2002
Published 22 November 2002
Online at stacks.iop.org/JPhysCM/14/13319

Abstract
Experimental results show that the free carrier mobility in AlGaN/GaN quantum wells strongly decreases with the carrier density. Using the dynamical theory, we show that this behaviour can be explained by a combination of phonon, carrier–carrier and interface defect scattering mechanisms.

(Some figures in this article are in colour only in the electronic version)

1. Introduction

Heterostructures of the wurtzite nitride family are in a quite unique position, since their (0001) interfaces are expected to bear a surface charge σ_0 resulting from the difference between the polarizations of the two alloys that are building the interface [1]. The spontaneous charge may be increased because of a strong piezoelectric response taking place in the strained cap layer [2–6]. For given set-ups, this charge creates an attractive potential and therefore a quantum well whose filling by free carriers results from the electronic dielectric response of the whole system (figure 1). The (screening) free electrons come either from the ionization of surface states or from bulk states. It can be shown experimentally that one does not need any intentional doping of the cap layers to obtain free carrier densities as large as several 10^{13} cm^{-2}—opposite to the case of quantum wells in the GaAs family, in which densities are generally limited to 10^{11}–10^{12} cm^{-2}. This particular situation has stimulated the interest from the device industry since a larger density of free carriers with a lack of scattering by doping ionized impurities should lead, in principle, to a large conductivity and therefore to good device performances. However, for obtaining increasing free carrier densities in the quantum well, it is necessary to combine an increase of the thickness of the AlGaN layer with use of increasing x compositions of the $Al_xGa_{1-x}N$ alloy. As a result, experimental measurements of transport properties obtained on LP MOVPE AlGaN/GaN heterostructures [7] clearly show that the carrier mobility μ severely decreases with the cap layer thickness and/or the x-value. More generally, collecting on the

[4] Author to whom any correspondence should be addressed.

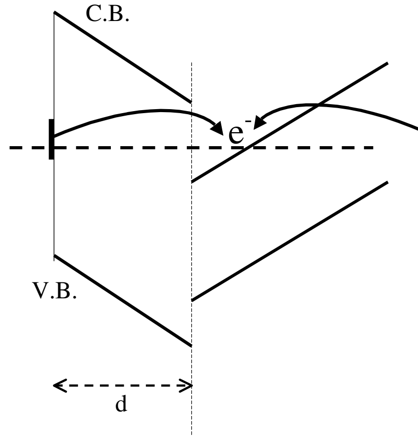

Figure 1. A schematic representation of an AlGaN/GaN triangular potential.

same curve all the points μ versus the carrier density n_s obtained for various samples (differing in their AlGaN thickness or x-composition), we observe a severe decrease of the mobility with increasing 2D carrier density (see figure 2). This mobility decrease may result from intrinsic mechanisms but also from the fact that the thicker the cap layer or the higher the x-value of the alloy composition, the higher the elastic energy stored in the cap layer. As a consequence, once a certain critical elastic energy limit is reached, it may induce strain relaxation mechanisms: the appearance of dislocations, interface roughness, but also, in the case of the structures presented in figure 2, the appearance of more and more V-shaped nano-holes and nano-trenches as seen by AFM [8]. This therefore creates new material-related (extrinsic) scattering mechanisms [7, 8]. The aim of this paper is to show that the experimental results may be theoretically recovered mainly by a combination of phonon, carrier–carrier and 'interface roughness-related' scattering mechanisms.

2. The theoretical framework

2.1. Use of the dynamical theory

For the low-field transport calculations, we have used the extension of the dynamical transport theory [9] to the case of a multi-occupied sub-band 2D system, with multi-sub-band screening included. In this approach [10], the collision time for isotropic scattering potentials is given by

$$\frac{1}{\tau_n^{\pm}(\vec{k})} = \frac{2\pi}{\hbar} e^2 B^{\pm} \sum_{n',k'} |\langle n, k | V^{tot}(r, \pm\omega) | n', k' \rangle|^2 (1 - \cos(\vec{k}, \vec{k}')) \delta[\varepsilon_{n'}(k') - \varepsilon_n(k) \pm \hbar\omega] \tag{1}$$

with $\vec{k}' = \vec{k} \mp \vec{q}$ and where

$$B^{\pm} = \mp \frac{f_0(\varepsilon_k \mp \hbar\omega) - f_0(\varepsilon_k)}{\hbar\omega(\partial f_0/\partial\varepsilon)_{\varepsilon_k}}. \tag{2}$$

The signs + or − stand respectively for emission or absorption processes. $V_{tot}(r)$ is the total scattering potential, with screening effects included, as indicated by the subscript 'tot'. The subscripts n and n' denote the various sub-bands. In the case of elastic potentials (ionized impurities, acoustic phonons, ...), the scattered electrons conserve their energy as well as

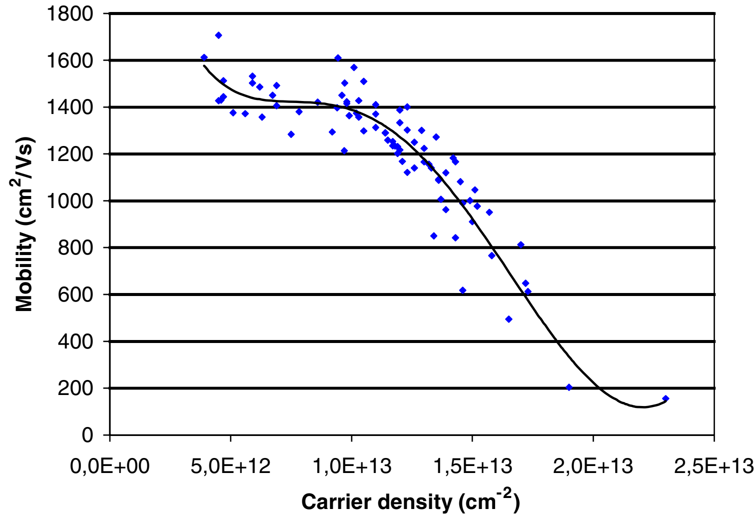

Figure 2. Room temperature mobility versus carrier density. The points were obtained for various AlGaN/GaN quantum wells grown by LP-MOCVD. The full curve is the mean polynomial representative curve.

their momentum modulus. In such cases, expression (1) reduces to the classical Boltzmann relaxation time. Matrix elements entering (1) are screened scattering potentials calculated between the various eigenstates $|n, k\rangle$ of the quantum well. In the case of multi-sub-band screening, they are given by [10]

$$\langle n, k|V^{tot}(r, \pm\omega)|n', k'\rangle = \delta_{k',k\mp q} \int Z_n^*(z) Z_{n'}(z)) V^{tot}(q, z, \pm\omega)\, \mathrm{d}z = \delta_{k',k\mp q} M_{n,n'}^{tot}(q, \pm\omega) \tag{3}$$

where the various $M_{n,n'}^{tot}(q, \pm\omega)$ are solutions of the following set of linear equations:

$$\sum_{m,m'} \varepsilon_{n,n'}^{m,m'}(q, \pm\omega) M_{m,m'}^{tot}(q, \pm\omega) = M_{n,n'}^{ext}(q, \pm\omega). \tag{4}$$

The unscreened potential matrix elements $M_{n,n'}^{ext}(q, \pm\omega)$ have the same definition (2) as $M_{n,n'}^{tot}(q, \pm\omega)$. The approximated expressions for the dielectric tensor components can be obtained in the form

$$\varepsilon_{n,n'}^{m,m'}(q, \omega) = \delta_{n,m}\delta_{n',m'} + \frac{k_{SC,m}(\omega)}{q}\delta_{n,n'}\delta_{m,m'}. \tag{5}$$

A set of screening wavevectors $k_{SC,m}$ are then defined and are given, in the case of static screening, by

$$k_{SC,m}(0) = \frac{m^* e^2 f(\varepsilon_m)}{2\pi\hbar^2 \varepsilon_L}. \tag{6}$$

3. Numerical determination of the quantum well energy states

Generally, the wavefunctions chosen for the evaluation of the various matrix elements are trial analytical functions [7, 11, 12] which, in practice, only allow the description of the first sub-band. In order to simulate the quantum well mobility and to check the effect of the

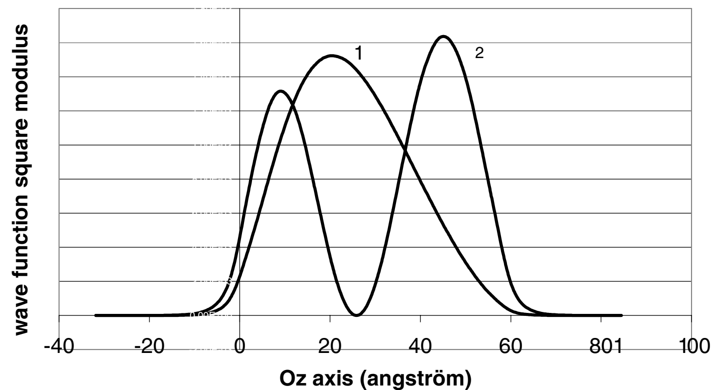

Figure 3. Wavefunction squared moduli of the two first energy states calculated for an $Al_xGA_{1-x}N/GaN$ quantum well with $x = 0.3$ and assuming that the interface charge σ is equal to the electronic density n_s.

carrier confinement on the various scattering mechanisms we have determined numerically the energy states and their associated wavefunctions, adapting methods usually used in *ab initio* calculations to the establishing and resolution of the envelope function equation [13]. Owing to the particularly large electronic density within the wells, the Coulomb interaction as well as the exchange and correlation contributions were introduced in the Kohn–Sham-like envelope function equation. Since the quantum well states are localized, it is assumed, in our numerical method, that they vanish at the extremities of a segment of length L in which the quantum well potential is embedded. Thus, the wavefunctions may be expressed as a Fourier series of planes waves that are naturally defined by the segment length L. In this plane-wave basis, the envelope function equation transforms into a matrix where the Coulomb as well as the exchange and correlation potentials are automatically calculated using the fast Fourier transform technique. The Kohn–Sham matrix eigenelements are then numerically solved using an iterative procedure and their eigenvalues allow us, finally, to calculate the full quantum well energy $E_T(L)$ which turns out to be a function of the parameter L. This last value L is chosen so as to minimize E_T. This variational procedure, already used in [14, 15], allows one to get precise numerical results with a relatively low number of plane waves (~50 in the present 1D localized case). Figure 3 illustrates the first two wavefunctions found in the case of the triangular potential shown in figure 1. Numerical results indicate that:

(i) for low carrier densities, more than one sub-band is significantly occupied by electrons, justifying the multi-sub-band formalism for the low-field transport calculation, with multi-sub-band screening effects included;
(ii) an increasing carrier density leads to a stronger confinement of the electronic density which is pushed towards the interface;
(iii) the Fermi level is strongly pushed upward to large energy values and exceeds 90 meV above the first energy ground state as soon as the carrier density exceeds $\sim 8 \times 10^{12}$ cm^{-2} (note that this particular value corresponds to the optical phonon energy).

4. Scattering mechanisms

We have introduced, in the present calculation, scattering mechanisms associated:

(i) with a possible distribution of ionized impurities within or outside the quantum well;

(ii) with threading dislocations (the Coulomb potential associated with a possible dislocation charge and the scattering potentials associated with the dislocation strain field);
(iii) with acoustic phonons interacting with electrons through the deformation potential and piezoelectric coupling;
(iv) with optical phonons interacting with electrons through their polar optical potential;
(v) with carrier–carrier scattering;
(vi) with interface roughness.

The two first types of scattering potential are quite standard and their 2D associated collision times can be straightforwardly derived from the well known 3D formulations [16, 17]. They will not be described in this paper. Although phonon scattering potentials are also well known in the 3D systems, the electron localization along the Oz axis in the case of quantum well leads to particular effects that we will underline in the following section. We also describe the carrier–carrier scattering since we make use of a slightly modified version of the Episov and Levinson formulation [18, 19]. Finally, in the particular case of triangular quantum well potentials, the description of interface roughness scattering is not obvious and we shall detail our approach in the following.

4.1. Phonon scattering

Although in 2D systems the phonon field may be different from that of 3D systems, it is generally assumed, for scattering calculation purposes, that it is sufficient to consider the 2D electrons as interacting with a 3D (unperturbed) phonon field. We use also this substantially simplifying approximation. In this case, acoustic as well as optical phonons interact with the carriers through potentials of the form

$$V_{ph,\kappa}(\vec{r}) = A(\kappa,\omega)(a_\kappa \mathrm{e}^{-\mathrm{i}\vec{\kappa}\cdot\vec{r}} + a_\kappa^+ \mathrm{e}^{\mathrm{i}\vec{\kappa}\cdot\vec{r}}) \tag{7}$$

where κ is the 3D phonon momentum, a and a^+ are annihilation and creation operators. The various functions $A(\kappa,\omega)$ depend on the phonon/electron coupling mechanisms and can be found in Ridley's book [16]. Such potentials (7) connect the electron and phonon systems, so their matrix elements have to be calculated connecting eigenstates corresponding, at first order, to the direct product of independent electron eigenstates $|n,k\rangle$ and independent phonon eigenstates $|n_\kappa\rangle$. In the particular 2D case, this gives, with $\langle r|n,k\rangle = (1/\sqrt{S})\exp(\mathrm{i}\vec{k}\cdot\vec{\rho})Z_n(z)$,

$$M_{n,n'}^{ext,\pm}(\vec{q},\omega) = A(\kappa,\omega)\left(\delta_{\vec{k}',\vec{k}\pm\vec{q}}\sqrt{n_\kappa + (1\pm 1)/2}\int_{-\infty}^{\infty} Z_n^*(z)Z_{n'}(z)\mathrm{e}^{\pm\mathrm{i}q_z z}\,\mathrm{d}z\right) \tag{8}$$

where we have introduced $\vec{\kappa} = (\vec{q}, q_z)$ and where $\vec{q} = \vec{k}' \mp \vec{k}$ is a 2D vector. n_κ corresponds to the Bose–Einstein occupation function. The screened matrix elements to be introduced in the collision time expression (1) are then solutions of equations (4) in which expressions (8) are introduced. It is worth noting that the final result will depend on the whole set of functions

$$I_{n,n'}^{\pm}(q_z) = \int_{-\infty}^{+\infty} Z_n^*(z)Z_{n'}(z)\mathrm{e}^{\pm\mathrm{i}q_z z}\,\mathrm{d}z \tag{9}$$

which are nothing else than Fourier transforms. These functions imply that the more confined the electronic density, the larger the phonon scattering effect: a consequence of the Heisenberg inequalities. This last remark constitutes the main difference between 2D and 3D electronic systems for phonon scattering.

4.2. *Carrier–carrier scattering*

This is essentially a two-particle process interacting through the Coulomb potential. Neglecting exchange contributions, we consider initial and final two-particle wavefunctions given by

$$|1,2\rangle = \frac{1}{S}Z(z)Z(z_2)\mathrm{e}^{\mathrm{i}(\vec{k}\cdot\vec{\rho}+\vec{k}_2\cdot\vec{\rho}_2)} \qquad |1',2'\rangle = \frac{1}{S}Z(z)Z(z_2)\mathrm{e}^{\mathrm{i}(\vec{k}'\cdot\vec{\rho}+\vec{k}'_2\cdot\vec{\rho}_2)} \tag{10}$$

with $\vec{r} = (\vec{\rho}, z)$. It is straightforward to show that the Coulomb potential matrix elements connecting such states are given by

$$\langle 1,2|\frac{e^2}{4\pi\varepsilon_0\varepsilon_L|\vec{r}_1-\vec{r}_2|}|1',2'\rangle = \frac{F_n(q)}{S^2\varepsilon_0\varepsilon_L q} \tag{11}$$

where we have introduced the form factor $F(q)$ given by [18, 19]

$$F_n(q) = \int \mathrm{e}^{-q|z-z_2|}|Z_n(z)|^2|Z_n(z_2)|^2\,\mathrm{d}z\,\mathrm{d}z_2. \tag{12}$$

The relaxation time may be obtained using (1) which has to be weighted in order to account for the occupation ratio of state 2 and empty-place ratio of state 2′. Introducing $\varepsilon_{k'_2} - \varepsilon_{k_2} = \hbar\omega$, this gives for each sub-band

$$\frac{1}{\tau_n(k)} = \frac{\pi e^4}{2(\varepsilon_0\varepsilon_L)^2\hbar S^2}\sum_{k',k_2,k'_2}\frac{f(\varepsilon_{k'})-f(\varepsilon_k)}{-\hbar\omega(\partial f/\partial\varepsilon)_k}\frac{F_n^2(q)}{q^2}\frac{\vec{k}\cdot\vec{q}}{k^2}\delta(\varepsilon_{k'}-\varepsilon_k-\hbar\omega)$$
$$\times\cdots\times f(\varepsilon_{k2})[1-f(\varepsilon_{k'_2})]. \tag{13}$$

It is hard to proceed further without any approximation. In order to find again the usual Episov and Levinson expression [19], we restrict the scattering processes to quasi-elastic collisions ($\omega \to 0$). This leads to

$$\frac{1}{\tau_n(k)} = -\frac{\pi e^4}{2(\varepsilon_0\varepsilon_L)^2\hbar S^2}\sum_{k',k_2}\frac{F_n^2(q)}{q^2}\frac{\vec{k}\cdot\vec{q}}{k^2}\delta(\varepsilon_{k'}-\varepsilon_k)f(\varepsilon_{k2})[1-f(\varepsilon_{k_2})]. \tag{14}$$

Expression (14) disconnects the sums over k' and k_2. The sum over k_2 can be exactly calculated in 2D systems and gives

$$\sum_{k_2} f(\varepsilon_{k_2})[1-f(\varepsilon_{k_2})] = \frac{KTm^*S}{2\pi\hbar^2}(1-\exp(-\pi\hbar^2 n_n/m^*KT)) \tag{15}$$

where n_n is the electron density of sub-band n. Transforming the sum over k' appearing in (14) into an integral, this gives

$$\frac{1}{\tau_n(k)} = \frac{m^{*2}KTe^4}{16\pi^2(\varepsilon_0\varepsilon_L)^2\hbar^5}(1-\exp(-\pi\hbar^2 n_n/m^*KT))\int_0^{2\pi}\frac{F_n^2(q)}{q^2}(1-\cos\theta)\,\mathrm{d}\theta. \tag{16}$$

Note that this last expression exactly coincides with the Episov and Levinson formula as soon as one makes the approximation $1-\exp(-\pi\hbar^2 n_n/m^*KT) \cong \pi\hbar^2 n_n/m^*KT$. However, the use of (16) leads to larger and more realistic mobility values.

4.3. *Interface roughness scattering*

Generally, the interface roughness scattering potential amplitude V_0 in square quantum wells is approximately determined by assuming that locally, the fluctuation of the interface position z of a quantity b (the roughness amplitude) shrinks the well width. Thus, assuming an infinitely deep potential of width L, this leads to a modification of the fundamental ground state of the quantum well given by $V_0 = \mathrm{d}\varepsilon_1 \cong \mathrm{d}(\hbar^2\pi/2m^*L^2) = -\hbar^2\pi b/4m^*L^3$. Obviously, this

method can no longer be used for triangular quantum wells, where, in a first approximation, the interface roughness only shifts the potential by a distance b: $V(z) \to V(z-b)$. To solve this particular problem, we may attribute to each point (x, y) a probability $P_b(x, y)$ that the interface is shifted by a distance b. Thus the Hamiltonian of the quantum well in the presence of interface roughness is given by

$$H_{QW} = \frac{p^2}{2m^*} + V(z) + (V(z-b) - V(z))P_B(x, y) = H_{0,QW} + W(x, y, z). \tag{17}$$

The $W(x, y, z)$ operator represents the interface roughness scattering potential. As long as this term constitutes a perturbation of the perfect QW Hamiltonian, its matrix elements (entering the definition of the collision time) may be calculated connecting the eigenstates of the perfect QW Hamiltonian. This gives

$$\begin{aligned} W_{n,n}(q) &= \frac{1}{S}\int \mathrm{e}^{-\mathrm{i}\vec{k}\cdot\vec{\rho}}|Z_n(z)|^2 W \mathrm{e}^{\mathrm{i}\vec{k}'\cdot\vec{\rho}}\,\mathrm{d}x\,\mathrm{d}y\,\mathrm{d}z \\ &= \frac{1}{S}P_b(q)\int_{-\infty}^{\infty}|Z_n(z)|^2(V(z+b) - V(z))\,\mathrm{d}z. \end{aligned} \tag{18}$$

Since the quantum well potential as well as its wavefunctions $Z_n(z)$ are known, the integral $V_n = \int |Z_n(z)|^2(V(z+b) - V(z))\,\mathrm{d}z$ entering (18) can be determined numerically. The remaining $P_b(q)$ term is the Fourier transform of the probability $P_b(x, y)$ which, using a standard result of statistical physics, may always be expressed in the form [20]

$$P_b(q) = S_b \exp\left(\sum_n \frac{(\mathrm{i}q)^n}{n!}C_n\right) \tag{19}$$

where $C_n = \langle\rho^n\rangle - \langle\rho\rangle^n$ with $\langle\rho^n\rangle = \int \rho^n P_b(\rho)\,\mathrm{d}x\,\mathrm{d}y$ and where S_b is a normalizing factor. In the case where the interface roughness is isotropic, only the C_{2n} coefficients do not vanish so, if we limit the sum to the second-order term in (19), we obtain [10, 21, 22]

$$P_b(q) = S_b \mathrm{e}^{-q^2 d^2/4} \to P_b(\vec{\rho}) = \frac{S_b}{\pi d^2}\mathrm{e}^{-\rho^2/d^2} \tag{20}$$

where we have introduced a correlation length $d = \sqrt{2C_2}$ in order to recover a usual correlation function (corresponding to the reversed Fourier transform of $P_b(q)$ also shown in 14). The above definition also implies that $S_b = \int P_b(\vec{\rho})\,\mathrm{d}^2\rho$ represents the area where the interface has been shifted. Introducing (20) into (18) we find

$$W_{n,n}(q) = \frac{S_b}{S}V_n \mathrm{e}^{-q^2 d^2/4} = \phi V_n \mathrm{e}^{-q^2 d^2/4} \tag{21}$$

where ϕ is a 'roughness' covering ratio.

5. Theoretical results and discussion

The total effect of acoustic and optical phonon scattering is illustrated in figure 4 (full curve with black squares). It leads to mobility values which strongly decrease with increasing carrier density. This strong decrease is a consequence of the progressive spatial localization of the electronic density which allows a larger and larger uncertainty in the electron momentum Oz component and therefore a larger and larger phonon contribution to the 2D electron scattering events. Moreover, increasing the carrier density also leads to a higher location of the Fermi level which reaches values (over the first sub-band ground state energy) larger than the optical phonon energy as soon as the carrier density reaches $\sim 8 \times 10^{12}$ cm^{-2}. Thus more and more optical phonon emission processes are possible and also the contributions to the free carrier mobility decrease.

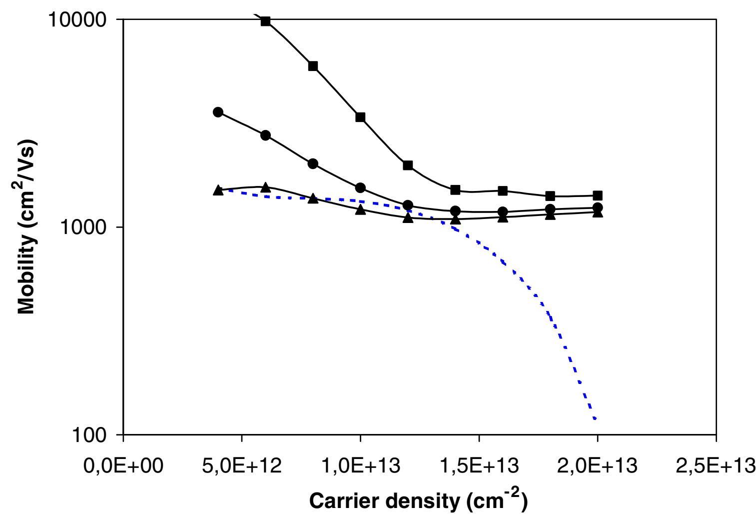

Figure 4. Theoretical calculation of the mobility at 300 K. The dashed curve is the mean polynomial representative curve for the experimental points. The full curve with black squares represents the role of acoustic and optical phonon scattering. The full curve with black circles represents the combined effect of phonon and carrier–carrier scattering. The full curve with black triangles represents the combined effect of phonon, carrier–carrier, impurity ($N_D = 4 \times 10^{18}$ cm^{-3}) or dislocation ($N_{dislo} = 10^{10}$ cm^{-2}) scattering.

When the carrier–carrier scattering is also taken into account, it leads to results shown in figure 4 (full curve with black circles). Such results include all the intrinsic (unavoidable) mechanisms and explain the regular decrease of the mobility. When the carrier density reaches values as large as 1.3×10^{13} cm^{-2}, the mobility values tend approximately towards a constant of the order of 1100 cm^2 V^{-1} s^{-1}. In principle this value should constitute the maximum mobility of the quantum well at large carrier densities. Comparing to the experimental results shown in figure 4 (dashed curve), it is clear that the combined phonon and carrier–carrier scattering mechanisms do not explain by themselves either the saturation of mobility obtained at low carrier concentration or the very sharp decay of the mobility that starts at carrier concentrations of 1.4×10^{13} cm^{-2}.

Introducing impurity scattering in the calculation provides the possibility of decreasing the mobility but only in the range of low carrier concentrations (figure 4, full curve with black triangles). However, to obtain values of the order of the experimental ones, it would be necessary to introduce ionized impurity densities as large as 4×10^{18} cm^{-3} which is an unrealistic value. Moreover, due to the increase of the screening effects with increasing carrier density, impurity scattering becomes negligible compared to intrinsic scattering. Thus, the strong mobility decrease observed at large carrier densities cannot be assessed for ionized impurities.

Threading dislocation scattering effects (with core charge potential and deformation potentials included) are quite similar to those of ionized impurities since they may only lead to an observable decrease of the mobility in the low-carrier-density range. Their scattering effect also becomes negligible compared to phonon effects when the free carrier density (and therefore the screening effect) increases. The only noticeable effect is obtained when the threading dislocation density reaches a value much larger than 10^{10} cm^{-2} which also constitutes an unrealistic value for our samples, in which the density is about 5×10^9 cm^{-2}.

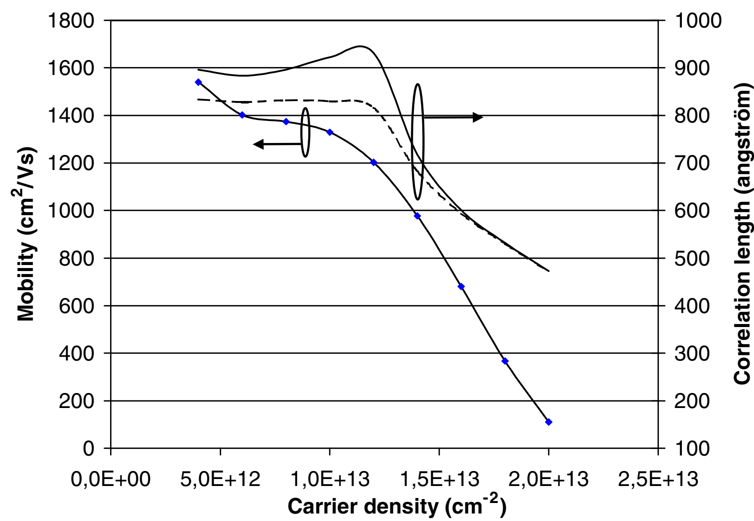

Figure 5. The exact theoretical fit of the tendency experimental curve (full curve with black squares), obtained by adjusting just the correlation length describing the interface roughness. The dashed curve represents the correlation length values when only phonon scattering mechanisms and interface roughness are considered. The full curve represents the correlation length when phonon and carrier–carrier scattering mechanisms are combined with the interface roughness.

Unlike those for the previous scattering centres (ionized impurities and dislocations), the interface roughness scattering mechanisms are efficient in the low-and in high-free-carrier-density ranges. The right order of magnitude for the low-carrier-density range is found for covering factors ϕ of the order of 0.5 and correlation lengths of the order of $\sim$90 nm (although, obviously, other (ϕ, d) couples of values may be chosen).

Considering then, phonon, carrier–carrier and interface roughness mechanisms only, we were able to reconstitute the tendency curve for the experimental results (figure 5, full curve with black squares) by just adjusting the correlation length. For example, the dashed curve in figure 5 represents the correlation length obtained by combining the phonon scattering with the interface roughness scattering, while the full curve corresponds to the correlation length obtained when phonon and carrier–carrier scattering are combined with the interface roughness scattering. It is worth noting that the whole tendency curve may be fitted with a constant correlation length up to the carrier density $\sim 10^{13}$ cm^{-2} and then with a regularly decreasing correlation length. This decrease reflects therefore interface quality degradation with increasing AlGaN thicknesses and/or the alloy composition x.

Finally, it is worth mentioning that the correlation function chosen to describe the interface roughness may also be used for any other kind of interface defect and, in particular, the nano-defects observed in the AlGaN top surfaces of the 2DEG structures [7]. Only the prefactor V_n would depend on the exact nature of the interface defects involved. However, numerical calculations show that the results are not so sensitive to this V_n-factor but much more to the correlation length d. Thus, instead of an interface 'geometrical' roughness, a lot of other 'exotic mechanisms'—for example, cracks appearing at the AlGaN layer or misfit dislocation tangles randomly distributed at the interface and randomly modifying the interface areal electrical charge (leading thus to a sort of interface 'electrical' roughness)—may always be imagined. Thus the effect of interface 'geometrical' roughness constitutes only one possibility that may explain the strong mobility decay. We therefore suggest that

the experimental mobility behaviour versus carrier density corresponding to increased Al% or AlGaN thickness is consistent with both:

(i) a progressive degradation of the interface (electrical or geometrical) quality;
(ii) an increasing effect of inhomogeneous scattering mechanisms induced by the AlGaN quality degradation.

Acknowledgment

This work was supported by the European Space Agency in the framework of ATHENA (ESTEC-contract 1405/00/NL/PA)

References

[1] Bernardini F, Fiorentini V and Vanderbilt D 1997 *Phys. Rev.* B **56** R10024
[2] Smorchkova I P, Elsaas C R, Ibbetson J P, Vetury R, Heying B, Fini P T, Haus E, DenBaars S P, Speck J S and Mishra U K 1999 *J. Appl. Phys.* **86** 4520
[3] Garrido J A, Sanchez-Rojas J L, Jiménez A, Munoz E, Omnes F and Gibart P 1999 *Appl. Phys. Lett.* **75** 2407
[4] Ibbetson J P, Fini P T, Ness K D, DenBaars S P, Speck J S and Mishra U K 2000 *Appl. Phys. Lett.* **77** 250
[5] Ridley B K, Ambarer O and Eastman L 2000 *Semicond. Sci. Technol.* **15** 270
[6] Ambarer O, Foutz B, Smart J, Shealy J R, Weimann N G, Chu K, Sierakowski A J, Schaff W J, Eastman L F, Dimitrov R, Mitchell A and Stutzmann M 2000 *J. Appl. Phys.* **87** 334
[7] Bougrioua Z, Farvacque J-L, Moerman I and Carosella F 2001 *Phys. Status Solidi* b **228** 625–8
[8] Bougrioua Z, Moerman I, Nistor L, Van Daele B, Monroy E, Palacios E T, Calle F and Leroux M 2002 *EXMATEC* (May 2002) at press
[9] Farvacque J-L 2000 *Phys. Rev.* B **62** 2536
[10] Farvacque J-L 2002 at press
[11] Ando T, Fowler A B and Stern E 1982 *Rev. Mod. Phys.* **54** 437
[12] Ridley B K, Foutz B E and Eastman L F 2000 *Phys. Rev.* B **61** 16862
[13] Farvacque J-L and Bougrioua Z 2002 at press
[14] Brinkmann D 1995 *Diplomarbeit* University of Grenoble
[15] Farvacque J-L and François P 2001 *Phys. Status Solidi* b **223** 635
[16] Ridley B K 1993 *Quantum Processes in Semiconductors* 3rd edn (Oxford: Clarendon)
[17] Farvacque J-L, Bougrioua Z and Moerman I 2001 *Phys. Rev.* B **63** 115202
[18] Episov S E and Levinson I B 1986 *Zh. Eksp. Teor. Fiz.* **90** 330
[19] Ridley B K and Zakhleniuk N A 2001 *Int. J. High Speed Electron. Syst.* **11** 479
[20] Reichl L E *A Modern Course in Statistical Physics* (London: Edward Arnold)
[21] Bougrioua Z, Farvacque J-L and Ferré D 1996 *J. Appl. Phys.* **79** 1536–45
Bougrioua Z, Farvacque J-L and Ferré D 1996 *J. Appl. Phys.* **79** 1546–55
[22] Penner U, Rücker H and Yassievich I 1998 *Semicond. Sci. Technol.* **13** 709